

Cite this: *J. Mater. Chem. C*,
2024, 12, 15654Received 25th July 2024,
Accepted 7th August 2024

DOI: 10.1039/d4tc03175j

rsc.li/materials-c

Bis(corannulyl)ethene as an efficient photochromic material†

Ryuta Imai, Shouhei Katao, Fumio Asanoma, Tsuyoshi Kawai * and
Mihoko Yamada *

We herein report photochromic 1,2-bis(2-methoxy-corannulyl)perfluorocyclopentene (**1**) possessing two corannulene moieties as the side aryl units of diarylethene. One enantiomer and the other enantiomer of one chiral atropisomer of **1** respectively forming columnar structures in the crystal were revealed *via* single-crystal X-ray analysis. Compound **1** exhibited an efficient photochromic behaviour with a large molar absorption coefficient of $5.0 \times 10^4 \text{ M}^{-1} \text{ cm}^{-1}$, and significantly high photochemical quantum yields of 0.64 and 0.49 were demonstrated for photocyclization and photocycloreversion reactions, respectively. This high efficiency was rationalized by the changed abundance ratios of atropisomers between the open- and closed-isomers and the shortened distance between reactive carbons with the help of the curved structure. In addition, the application possibility of **1** as a photochromic material was demonstrated in a poly(methyl methacrylate) film.

Introduction

Photochromic compounds, which exhibit reversible colour change accompanying isomerization through photoirradiation, have attracted much attention and have been broadly studied for the development of material functions such as sensing, optical memory, and photo-switching.^{1–6} Among them, diarylethenes and related substances are intensively studied owing to their high durability and high thermal stability.^{1,7,8} They undergo photocyclization from open-form to closed-form isomers under UV irradiation and photo-cycloreversion under visible-light irradiation. Their practical photo-sensitivity is enhanced by increasing optical absorbance and photochemical quantum yields. For example, the photocyclization quantum yield is increased by controlling the conformation of open-form isomers,⁹ *i.e.*, the photoreactive anti-parallel conformation

should be highly photosensitive but the parallel one is photochemically non-reactive because photocyclization proceeds through a symmetry-allowed conrotatory pathway.⁸ In the photochromism of diarylethenes, both photocyclization and photocycloreversion proceed through the same conical intersection to the ground state. Hence, the sum of the quantum yield values of photocyclization ϕ_{o-c} and photocycloreversion ϕ_{c-o} should be unity at the maximum.¹ A simultaneous increase in ϕ_{o-c} and ϕ_{c-o} is thus challenging for exploring efficient colour-changing and photo-switching molecular materials. In this regard, our strategy is to exploit the curved aromatic structure of diarylethenes to perturb the ground-state structure of open and closed isomers and reaction pathways of forward and reverse reactions. Corannulene,^{10–15} a bowl-like curved aromatic compound, has attracted significant interest owing to its large curved π -surface with some unique features such as geometrical and electronic anisotropy,^{14,16,17} characteristic bowl-to-bowl inversion,^{18–20} large HOMO–LUMO gap,²¹ and formal 20π electrons, which are much different from those of classic planar $4n + 2\pi$ aromatic compounds.^{13,22}

We have recently reported tetrathienyl corannulenes with a high photocyclization quantum yield, close to unity.²³ It further displayed high photosensitivity with a large absorption coefficient in the UV range, which is mainly because of the central corannulene unit.

Herein, we report a diarylethene derivative with two corannulene moieties as side aryl units and its photochromic behaviour together with a discussion on its atropisomers.

Division of Materials Science, Graduate School of Science and Technology, Nara Institute of Science and Technology (NAIST), Ikoma, Nara, 630-0192, Japan.

E-mail: myamada@ms.naist.jp

† Electronic supplementary information (ESI) available: Synthetic procedures, ¹H, ¹³C and ¹⁹F, and variable-temperature NMR (Fig. S1, S2 and S6–S8), EI mass (Fig. S3), GPC (Fig. S4), crystallographic parameters (Table S1), the intermolecular interactions (Fig. S5), DFT-predicted optimized structure (Fig. S9), MOs (Fig. S10 and S11), NICS(0) values (Fig. S12), absorption spectra (Fig. S13 and S14), Emission spectra (Fig. S15), UV-vis and NMR spectral change (Fig. S16, S18 and S19) and repeated durability (Fig. S17). Conformations of **1o-1** (Fig. S20), photo-reaction quantum yields (Table S2) and Arrhenius plot and Eyring plot (Fig. S21). UV-vis spectral change of the films (Fig. S22 and S23) and PXRD pattern (Fig. S24). CCDC 2345853. For ESI and crystallographic data in CIF or other electronic format see DOI: <https://doi.org/10.1039/d4tc03175j>



Results and discussion

Synthesis and characterization of a bis(corannulenyl)ethene compound

1,2-Bis(2-methoxy-corannulenyl)perfluorocyclopentene (**1**), a new diarylethene derivative with two curved aromatic corannulene units as side aryls, was designed and synthesized *via* the coupling reaction of 1-bromo-2-methoxycorannulene and perfluorocyclopentene in 16% yield (Fig. 1). **1** was characterized using ^1H , ^{19}F and ^{13}C NMR spectroscopy (Fig. S1 and S2, ESI †) and EI mass spectrometry (Fig. S3, ESI †).

The isolation of **1** was confirmed on the GPC profile (Fig. S4, ESI †), NMR and MS. The ^1H NMR spectrum of **1** showed signals of aromatic/aliphatic region in 16:6 ratio in both CDCl_3 and toluene- d_8 . The two characteristic methyl peaks suggested the C_s -symmetric parallel and the C_2 -symmetric anti-parallel conformations (see also Fig. S1 and S2, ESI †), with their ratios of about 1:5 and 1:8 in CDCl_3 and toluene- d_8 , respectively. The minor signals in the aromatic region were also assigned to the parallel conformation. The major component of the C_2 -symmetry was clearly confirmed with the single 2F peak of the central CF_2 unit in the ^{19}F NMR spectra (Fig. S1c and S2b, ESI †), while those of the minor component displayed geminal splitting in the C_s -symmetry. An EI mass signal assigned to $[\mathbf{1}]^+$ was observed at $m/z = 732.1524$.

Crystal structure of **1**

A colourless needle crystal suitable for single-crystal X-ray analysis was obtained by the slow evaporation of a solution of **1** in CH_2Cl_2 . The molecular structure and crystallographic parameters of **1** are shown in Fig. 2a and Table S1 (ESI †), respectively. The depth of the corannulene moiety of 0.092 nm is similar to that of the non-substituted corannulene (0.087 nm),¹¹ which may be influenced by the crystal packing with intermolecular interactions.²⁴ The crystal is composed of a couple of enantiomers of C_2 -symmetric anti-parallel isomers (Fig. 2a). The two di-substituted curved corannulene moieties on each molecule have the same chirality based on their curvature, denoted as *P* and *M* in Fig. 2,²⁵ with unique helicity around the central hexatriene structure. *PP* and *MM* isomers were observed. The C–C distance between the reactive carbon atoms was 0.493 nm. The crystal showed no photochromism, as expected from the C–C distance that was much longer than 0.42 nm, which is not suitable for the photocyclization reaction in crystals.²⁶

In the crystal, corannulene moieties of the same *PP* or *MM* isomers are stacked enantiomerically with intermolecular

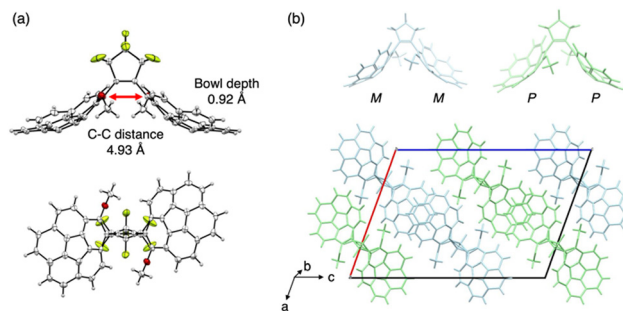


Fig. 2 Single-crystal X-ray structures of **1**. (a) Molecular structure represented with 50% thermal ellipsoids and viewed from the top (top) and the side (bottom) and (b) the packing structure.

$\text{CH}\cdots\pi$ interactions²⁷ and weak π - π interactions²⁸ in a concave-convex fashion, where the distances are 2.9 Å (< the sum of the van der Waals radii) and 3.8 Å, respectively, forming a columnar structure in a zig-zag manner (Fig. 2b and S5, ESI †). The other corannulene moieties of these molecules positioned outside of this columnar structure are also arranged in a similar zig-zag columnar manner so as to construct a 2D layer structure with single handedness. Such 2D layer structures respectively composed of *PP* and *MM* enantiomers are alternately arranged in an ABAB fashion with intermolecular $\text{CH}\cdots\pi$ and $\text{CH}\cdots\text{F}$ interactions²⁹ with the distances of 2.8 Å and 2.5 Å, respectively, shorter than the sum of the van der Waals radii. We also observed non-photochromic behaviour of the powdered sample prepared by grinding the crystals, which is tentatively ascribed to retention of the conformation with less photoactivity, as in the crystal structure.

Atropisomers of **1**

Variable-temperature NMR and DFT calculation were performed to examine the presence of atropisomers of **1**. The coalescence of the methyl peaks of parallel and antiparallel isomers with increasing temperature in variable-temperature NMR corresponded to the rotation of the corannulene groups (Fig. S6 and S8, ESI †). With decreasing temperature, the methyl peaks of parallel and antiparallel isomers broadened and split into at least three and two peaks, respectively. The parallel and antiparallel isomers appear to be composed of several atropisomers, which are distinguishable at a temperature lower than 203 K in CD_2Cl_2 or toluene- d_8 (Fig. S7 and S8, ESI †). The activation energy of the bowl-to-bowl inversion of the corannulene compound with the depth of 0.084 nm was reported to be 10.2 kcal mol $^{-1}$ with a coalescence temperature of 209 K.¹⁸ Considering the reported correlation between the depth and inversion¹⁰ and the depth of **1** in crystal, the observed coalescence at low temperature is attributed to the reduced inversion rate of corannulene and recognizable isomers based on its curvature.

We then studied the possible ground state structures of the open form of **1**, **1o** by means of DFT calculation at the $\text{wB97XD}/6\text{-}31\text{+G(d)}$ level. **1o** is able to have many atropisomers, based on the combination of central hexatriene structure, in

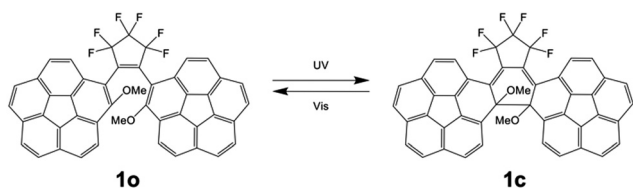


Fig. 1 Molecular structures of the open-form **1o** and the closed form **1c** in the photochromism of **1**.



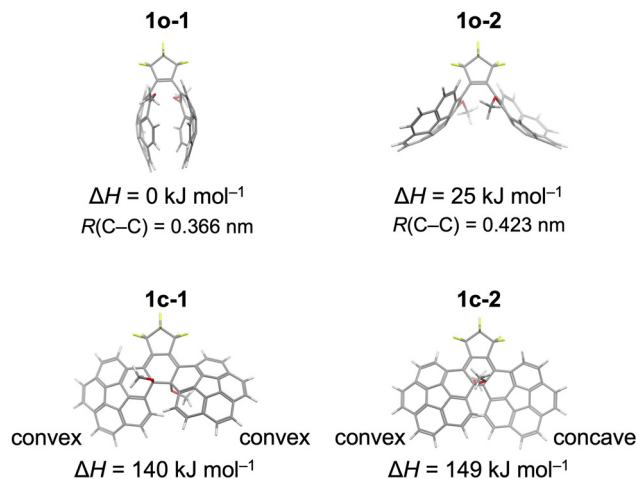


Fig. 3 Atropisomers of antiparallel open-form isomers of **1o-A**, **1o-1** and **1o-2** and closed-form isomers **1c**, **1c-1** and **1c-2**. Enantiomers are omitted for clarity.

parallel and C_2 -symmetric anti-parallel isomers of **p** and **m** helicity. By counting bowl-shaped di-substituted corannulenes of *P* and *M* isomers, we could expect 4 parallel isomers and 8 anti-parallel isomers such as **PpP** and **PmP**. As the most stable isomer, we elucidated a possible structure of an anti-parallel isomer **1o-1** (Fig. 3), which is **PpP** of quasi C_2 -symmetry (and **MmM**, of course). The isomer **1o-1** displays the distance of 0.366 nm between the reaction centre carbon atoms, which is suitable for the photocyclization reaction. We could also evaluate the possible structure of **PmP** type C_2 -symmetric anti-parallel structure **1o-2**, which resembles the crystal structure (Fig. 2). Although **1o-2** is significantly (*ca.* 25 kJ mol⁻¹) higher than **1o-1** in energy, it seems to be stabilized in the crystal packing with inter-molecular interactions. We could also elucidate other possible structures for **1o**, as exemplified in the ESI† (see Fig. S9 and S10). Some of these isomers are possibly co-existing in the solution phase at ambient temperature. We also conducted DFT calculation for the closed-form isomer **1c**. As illustrated in Fig. 3, the most stable **1c-1** possesses **PmM** type non-symmetric structure. Quasi C_2 -symmetric structure **1c-2** is about 9 kJ mol⁻¹ higher than **1c-1** in energy. Although the origin of this considerable energy loss in **1c-2** is not fully revealed (see Fig. S9 and S11, ESI†), light irradiation would promote structural transformation between the quasi C_2 -symmetric **1o-1** and non-symmetric **1c-1** along with the bowl-to-bowl inversion and breaking the symmetry during or after the photoisomerization reaction. Hence, the forward and the backward photoisomerization reactions may proceed through different reaction pathways. The bowl-depth of **1c-1** (0.079 nm and 0.076 nm) are considerably shallower than that of normal corannulenes (0.084 nm) and **1o-1** (0.088 nm), which may decrease the NMR-coalescence temperature of **1c**. **1o/1c** were also characterized with their energy difference ΔH values of about 131–146 kJ mol⁻¹, which depend on the atropisomers. This relatively large energy change might be rationalized with the difference in the aromatic stabilization in the corannulene units in **1o/1c**. We investigated the change in the

aromaticity upon photocyclization by means of the NICS(0)^{30,31} values derived by the DFT calculations at the ω B97XD/6-31+G(d) level. Considerable positive change was elucidated in the NICS(0) value (Δ NICS(0)_{1c-1o} = +13.62 & +13.70) at the reaction centre C_6 rings of corannulene units (Fig. S12, ESI†). These computational results are apparently opposite to the primitive expectation for the corannulene units in **1o/1c**, which proceed to formal conversion between the 20 π non-aromatic and the 18 π aromatic systems.

The absorption spectra of the atropisomers of **1o** were also calculated by TD-DFT at the ω B97XD/6-31+G(d) level, which overlaps with the practically identical absorption maxima and intensities, which correspond to the observed spectra (Fig. S13, ESI†). The TD-DFT calculation was also performed to the atropisomers of **1c** (Fig. S14, ESI†), again suggesting the similar absorption bands. We analysed **1** as an ensemble of atropisomers due to the difficulty in separation, also considering the similarity in the absorption spectra.

Photochemical properties

The optical properties of **1o** were characterized with UV-vis absorption spectra and compared with those of typical diarylethenes (Table 1). In CHCl₃, compound **1o** showed an absorption band at 293 nm with a large absorption coefficient ϵ of 6.2×10^4 M⁻¹ cm⁻¹ as expected for its two corannulene skeletons. In toluene, the absorption band was almost the same at 294 nm with a smaller ϵ (5.0×10^4 M⁻¹ cm⁻¹). Slight solvent-dependent shift may suggest the CT character of the absorption, which changes the ϵ value by altering the overlap with shorter absorption bands.

Compound **1o** displayed fluorescence emission with a peak at 480 nm in toluene, where no significant effect of atmosphere was observed (Fig. S15, ESI†). The emission quantum yields ϕ_f of **1o** was 0.016 in toluene under excitation at 365 nm.

Photochromism of **1**

The colourless solution of **1** turned purple in colour upon UV-irradiation and this photochromic reaction was characterized with UV-vis absorption and ¹H NMR spectra. A CHCl₃ solution of **1o** was irradiated by UV light at 365 nm to show spectral change with the progressive absorption peak at 543 nm and shoulder peaks at about 350 and 400 nm, which are assigned to the closed form isomer **1c** (Fig. S16, ESI†). From the isosbestic point, this reaction appears to be a 1-to-1 reaction without any significant side reaction. The spectrum turned back to the original state by the successive visible-light irradiation, indicating photochromism between **1o** and **1c**. A toluene solution of **1o** also exhibited similar photochromic behaviour with the peak appearing at 546 nm and shoulders at about 350 and 400 nm and an isosbestic point at 303 nm by UV-irradiation (Fig. 4). The high durability was demonstrated by repeating the colouration and bleaching cycles at least 10 times without photodegradation (Fig. S17, ESI†).

Isomer **1c** was isolated as a dark purple solid by HPLC with CHCl₃:hexane = 1:3. The isolated **1c** showed UV-vis spectra with the peaks at 543 and 546 nm in CHCl₃ and toluene with shoulders at about 350 nm and 400 nm, respectively. Visible-light irradiation reproduced the spectra of **1o**. The ϵ value of **1c** was estimated to be 7.7×10^3 M⁻¹ cm⁻¹ at 543 nm in CHCl₃,



Table 1 Optical properties of **1** in toluene and literature values of **2–5** in *n*-hexane

Compound	Solvent	$\epsilon_o^a/M^{-1} \text{ cm}^{-1}$ ($\lambda_{\text{max},o}/\text{nm}$)	$\epsilon_c^a/M^{-1} \text{ cm}^{-1}$ ($\lambda_{\text{max},c}/\text{nm}$)	Φ_{o-c}	Φ_{c-o}
1	Toluene	50 100 (294)	6000 (546)	0.64	0.49
2 ^b	<i>n</i> -Hexane	6780 (245)	1040 (511)	0.017	0.35
3 ^b	<i>n</i> -Hexane	7650 (282)	7820 (480)	0.16	0.05
4 ^b	<i>n</i> -Hexane	25 000 (275)	3800 (581)	0.26	0.15
5 ^b	<i>n</i> -Hexane	33 000 (309)	15 000 (625)	0.44	$<2.0 \times 10^{-5}$

^a Absorption coefficients of the open and the closed forms of ϵ_o and ϵ_c are shown with the absorption maxima $\lambda_{\text{max},o}$ in the UV region and $\lambda_{\text{max},c}$ in the visible region, respectively. ^b The optical properties of **2–5** in *n*-hexane were reported in the literature.^{32–35}

and $6.0 \times 10^3 \text{ M}^{-1} \text{ cm}^{-1}$ at 546 nm in toluene (Table 1). The maximum conversion ratio was about 46% at photostationary state with irradiation at 300 nm in diluted toluene solution.

The photochromic behaviour of **1** was also investigated by ¹H and ¹⁹F NMR spectroscopy (Fig. S18 and S19, ESI†). New peaks appeared in both the aliphatic and aromatic region by UV-irradiation at 365 nm in CDCl₃ or in toluene-*d*₈, corresponding to the formation of **1c**. The NMR spectra returned to the original state by the following visible-light irradiation, which is consistent with the photochromic behaviour observed by the absorption spectra. The conversion ratio was estimated to 8% or 10% in CDCl₃ or toluene-*d*₈ in the NMR tube, respectively. **1c** displayed a single CH₃ signal at 2.54 ppm in CDCl₃, indicating the symmetric structure at ambient temperature, which was also supported by the ¹⁹F NMR spectra.

The photochemical quantum yields for photocyclization ϕ_{o-c} and cycloreversion ϕ_{c-o} were estimated to be 0.30 and 0.31, respectively, in CHCl₃. In toluene, interestingly, much larger values of $\phi_{o-c} = 0.64$ and $\phi_{c-o} = 0.49$ were obtained, indicative of the high efficiency of both photocyclization and photo-cycloreversion in a less polar solvent. The increase in the ϕ_{o-c} values with decreasing solvent polarity from CHCl₃ to

toluene may be partly ascribed to the twisted intramolecular charge transfer, similar to those of the previously reported diarylethenes.³⁶ We may also consider the solvent effect on the relative population of different isomers of both **1o** and **1c**. The DFT-predicted structures of **1o** in the planar conformation in the ground state (Fig. S20, ESI†) showed large and asymmetric dihedral angles and the C–C distance is close enough for photocyclization, possibly due to geometrical distortion and asymmetry. Even if both dihedral angles are supposed to be 90°, similar to that in the twisted conformation, photoreactive C–C distance would be less than 0.42 nm, suitable for photocyclization.²⁶ Such a geometrical distortion that originated from the corannulene curvature may be one reason for the high ϕ_{o-c} value. The ϕ_{o-c} value of 0.64 in toluene is more than double of 0.30 in CHCl₃. Since the ratio of the antiparallel conformer in CDCl₃ is almost the same as that in toluene-*d*₆, 83% (1 : 5) and 89% (1 : 8), respectively. The significant solvent effect should be explained by the solvent-dependent ϕ_{o-c} value of the reactive antiparallel conformer and the solvent-dependent abundance ratios of the several atropisomers associated with corannulene inversion.

While the methoxy groups on the reactive carbons strongly suppress the ϕ_{c-o} of dithienylethenes,³⁵ it increases the ϕ_{c-o} of diarylethene with naphthalene.³³ The present relatively large ϕ_{c-o} value of **1c/1o** might be related to the effect of methoxy group on the reactive carbons and, meanwhile, is the largest value so far reported for diarylethenes with methoxy groups. The ϕ_{c-o} value of 0.49 is almost comparable to the ϕ_{o-c} value of 0.64 as well as the ϵ value at the irradiation wavelength. Such comparable balance of both reactions results in the conversion ratio at the photostationary state of only 46% in spite of the high photosensitivity. We also confirmed no remarkable oxygen effect on the quantum yields, supporting singlet excited state on the dominant reaction pathway (Table S2, ESI†). The sum of the ϕ_{o-c} and ϕ_{c-o} values of **1o/c** reached 1.13, markedly beyond unity. This implies significant perturbation on the forward and reverse reaction pathway, which could originate from the interconversion between atropisomers in the ground and/or the excited states.

VT-NMR of the closed form **1c** interestingly showed no coalescence behaviour in the temperature range between

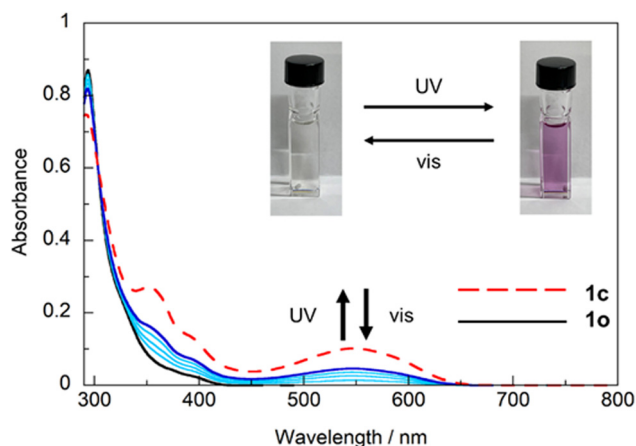


Fig. 4 The UV-vis absorption spectral change in **1o** in toluene under photoirradiation at 300 nm and the UV-vis absorption spectrum of **1c** with the colour change of the solution.



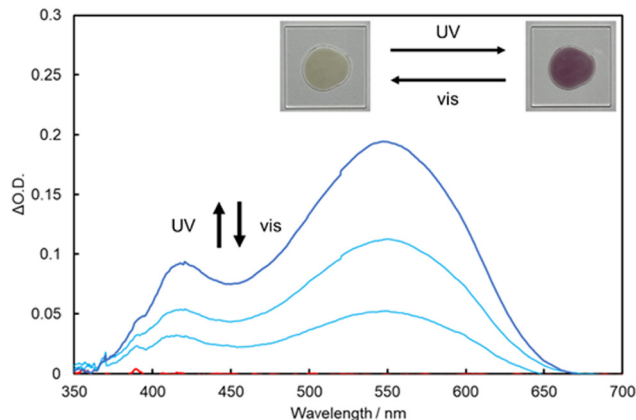


Fig. 5 The UV-vis absorption spectral change in a **1o**/PMMA film, prepared by drop-casting chloroform solution containing **1o** (12 mM) and PMMA (10 wt%) (**1o**/PMMA = ca. 5 wt%) under photoirradiation at 365 nm. Inset: Colour change of a **1o**/PMMA film.

183 K and 403 K, different from **1o**, which shows coalescence below 203 K (Fig. S6–S8, ESI[†]). The bowl-curvature becomes shallower upon photocyclization, as elucidated by DFT calculation, which should suppress the activation energy for the bowl-to-bowl inversion of corannulene units in **1c**.

Thermal stability of **1**

1c showed no marked fading at 363 K (90 °C) for 8000 s, which implies significantly high thermal stability in the closed form isomer. This is obviously contradictory to the relatively large energy difference between **1o** and **1c**, ΔH , of 140 kJ mol⁻¹ between **1o-1** and **1c-1**, for example (Fig. 3 and Fig. S9, ESI[†]). The thermal fading kinetics was evaluated between 403 K and 433 K for elucidating the activation energy of the cycloreversion reaction, $E_a = 89$ kJ mol⁻¹, with a frequency factor $A = 3.73 \times 10^7$ s⁻¹ obtained from the Arrhenius plot (Fig. S21b, ESI[†]).³⁷ The half-lifetime $t_{1/2}$ is calculated to be 4 years at 20 °C, which is sufficiently stable for classifying to the P-type photochrome. The very small A value, which is 10⁴–10⁶ times smaller than that of previously reported typical diarylethenes,^{38–40} should be responsible for the high thermal stability of **1c**. In addition, the thermodynamic activation parameters of enthalpy ΔH^\ddagger , entropy ΔS^\ddagger and Gibbs free energy ΔG^\ddagger were evaluated to be 85 kJ mol⁻¹, -111 J K mol⁻¹ and 119 kJ mol⁻¹, respectively, by the Eyring plot (Fig. S21c, ESI[†]). The large negative value of ΔS^\ddagger suggests that the degree of randomness affects the thermal stability, which may be ascribed to the atropisomers, their bowl inversion behaviour, or the increase of the bowl depth upon cycloreversion.

Photochromism of **1** in a film

We further demonstrated the photochromic feature of **1o/c** in poly(methyl methacrylate) (PMMA) films. The clear pale yellow film was prepared from the CHCl₃ solution of **1o** and PMMA by drop-casting and drying on a quartz plate. The PMMA film of **1o** exhibited photochromism with the increase in the absorption at 550 nm by UV-irradiation and the decrease in visible-light

irradiation (Fig. 5 and Fig. S22b, ESI[†]). No marked shift in the absorption bands from those in the solution was observed (Fig. S22a, ESI[†]). The durability of the film was confirmed by repeating the colouration and bleaching cycles for 10 times without marked photodegradation (Fig. S22c, ESI[†]). No marked change in the conversion ratio to **1c** was observed in the successive cycles. A weak emission was also observed similar to that in a solution (Fig. S22d, ESI[†]). The photochromic behaviour in the PMMA film indicated that **1o** could have a reactive conformation and the intermolecular packing effect should be suppressed.^{41,42}

We further assessed the neat film of **1o**, which was prepared by drop-casting the CHCl₃ solution of **1o**. It showed no colour change under UV-irradiation (Fig. S23a, ESI[†]). Powder X-ray diffraction showed diffused peaks, indicating a partially crystalline state (Fig. S24, ESI[†]). The diffraction peaks partly overlapped with the simulated ones for the single-crystal data, which suggested that a part of the structure in the bulk crystal could be maintained in the neat film. The apparent crystallite size D was calculated to be 20 nm by Scherrer's equation.⁴³ We also prepared a neat film of **1c** with deep purple colour. The absorption band at 550 nm decreased with visible-light irradiation but was not recovered under UV-irradiation (Fig. S23b, ESI[†]). The bleaching reaction seems to form **1o** with reactive anti-parallel conformation, which might spontaneously turn to the non-reactive conformation, possibly similar to those in the crystalline structure through the bowl-to-bowl inversion. To the best of our knowledge, the present results deliver the first example of the photoswitching nature of corannulene derivatives in neat films. One-way photoresponse behaviour has been studied for some applications such as imaging technology.^{44,45}

Compound **1** showed the following characteristics in solution and in a PMMA film: (i) high photoreactivity of both cyclization and cycloreversion reactions, $\phi_{o-c} = 0.64$ and $\phi_{c-o} = 0.49$, (ii) a very large molar absorption coefficient of the open isomer of 5.0×10^4 M⁻¹ cm⁻¹, (iii) large enthalpy difference between the open and closed form of more than 140 kJ mol⁻¹, (iv) the closed form displays significant thermal stability, which is partly because of the entropy effect and could be ascribed to the changes in the bowl-depth and to the possible bowl-to-bowl inversion upon isomerization. Because of the low frequency factor and modest activation energy, compound **1** behaves as the "P-type" photoswitching unit in a wide temperature range. These figures of **1** may also shed a light on the possible tunability of internal heat capacity and energy storage capability by means of curved aromatic units.^{46,47} These results thus suggest the unique functionality of curved aromatic units in photochromic units for various molecular materials, including photoswitching and light energy technology.

Conclusions

In conclusion, we synthesized herein a new diarylethene derivative **1** with two curved aromatic corannulene skeletons as the side aryl units and studied its photochromic behaviour.



Compound **1** showed high photochromic efficiency in toluene with a large ϵ value of the open form, $5.0 \times 10^4 \text{ M}^{-1} \text{ cm}^{-1}$, at 294 nm and large quantum yields of the photoreactions ($\phi_{o-c} = 0.64$ and $\phi_{c-o} = 0.49$). Interestingly, the sum of ϕ_{o-c} and ϕ_{c-o} values was >1.0 , which can be explained by the existence of atropisomers based on the curvature with different quantum yields and the change in their abundance ratio in **1o** and **1c** with the help of geometrical curvature. DFT calculation predicts reversible photomodulation in the bowl-depth of corannulene units. The high thermal stability of **1c** in spite of the large ϕ_{c-o} was explained by a significantly small frequency factor $A = 3.73 \times 10^7 \text{ s}^{-1}$ and a large negative value of $\Delta S^\ddagger = -111 \text{ J K mol}^{-1}$, even with a moderate activation energy in the ground state and a small activation energy in the excited state. In addition, the photochromism of **1** was demonstrated in PMMA films, while one-way colour change was observed in the bulk neat film. The high photosensitivity, large enthalpy difference and high thermal stability of **1** demonstrated promising properties based on the curved structure for future applications such as energy storage.

Experimental

Materials

Chemicals were purchased from FUJIFILM Wako Pure Chemical Corporation, Tokyo Chemical Industry Co., Ltd (TCI), Kanto Chemical Co., Inc. or Sigma-Aldrich Japan G.K. and used as received without further purification. Silica gel column chromatography was performed using silica gel 60N (spherical neutral, particle size 63–210 μm). Recycling preparative GPC separation was performed with a LaboACE LC-5060 (Japan Analytical Industry Co., Ltd).

Synthesis of **1**

1-Bromo-2-methoxycorannulene (360 mg, 1.00 mmol, 1.00 eq.) was dissolved in dry THF at -78°C under nitrogen. 1.6 M *n*-BuLi in hexane (660 μL , 1.05 mmol, 1.05 eq.) was slowly added and stirred for 3 h at -78°C . Then, 0.75 M perfluorocyclopentene in THF (530 μL , 0.40 mmol, 0.40 eq.) was gradually added dropwise. The mixture was stirred for 4 h at -78°C and then overnight at room temperature. The reaction mixture was poured into 1 M HCl (6 mL). The solution was extracted with CH_2Cl_2 (5 mL \times 2) and washed with water. The organic layer was dried over anhydrous MgSO_4 and the solvent was evaporated. After purification by silica gel column chromatography (Hexane : $\text{CH}_2\text{Cl}_2 = 5 : 1$), 1,2-bis(2-methoxy-corannuleny)perfluorocyclopentene (58 mg, 0.08 mmol, 16%) was obtained as a yellow solid. $^1\text{H NMR}$ (500 MHz, toluene- d_8): δ 8.08 (dd, $J = 2, 9 \text{ Hz}$, 2H, ap), 7.60 (d, $J = 9 \text{ Hz}$, 2H, ap), 7.43 (d, $J = 9 \text{ Hz}$, 2H, ap), 7.30 (d, $J = 9 \text{ Hz}$, 2H, ap), 7.23 (d, $J = 9 \text{ Hz}$, 2H, ap), 7.10 (d, $J = 9 \text{ Hz}$, 2H, ap), 6.88 (m, 4H, ap), 4.11 (s, 0.75H, p), 3.82 (s, 6H, ap). $^{19}\text{F NMR}$ (470 MHz, toluene- d_8): δ -107.53 (dd, $J = 9, 263 \text{ Hz}$, 0.3F, p), -108.99 (d, $J = 263 \text{ Hz}$, 2F, ap), -110.13 (d, $J = 263 \text{ Hz}$, 2F, ap), -111.92 (dd, $J = 9, 263 \text{ Hz}$, 0.3F, p), -131.84 (quin, $J = 6 \text{ Hz}$ 2F, ap), -131.5 – 133.2 (m, 0.3F, p). HRMS (EI) m/z : calcd for $\text{C}_{47}\text{H}_{22}\text{F}_6\text{O}_2$

$\{[\mathbf{1}]^+\}$: 732.1524; found: 732.1524. The peaks due to parallel and antiparallel conformations of **1** are denoted as p and ap, respectively.

NMR measurement

NMR spectra were recorded on a JEOL JNM-ECA600 (600 MHz), JEOL JNM-ECZ500R (500 MHz) or JEOL JNM-ECX400P (400 MHz). Compound **1** has two conformations, parallel (p) and antiparallel (ap). In the $^1\text{H NMR}$ spectra, the parallel peaks in the aromatic region were difficult to be identified because these are very small and overlapped with the antiparallel peaks. VT-NMR were measured in CD_2Cl_2 (183–293 K), tetrachloroethane- d_2 (293–403 K) and toluene- d_8 (183–373 K). The temperature was changed at 10 K and measurements were performed after the temperature had remained constant.

MS measurement

Electron Ionization (EI) mass spectra were recorded on a mass spectrometer (JEOL JMS-700 MStation for EI). The samples were prepared by dissolving in CHCl_3 .

Single-crystal X-ray analysis and powder X-ray diffraction

Single-crystal X-ray crystallographic analysis was performed using a Rigaku XtaLAB Synergy (1.2 kW) diffractometer with photon Jet-R rotating anode X-ray source $\text{CuK}\alpha$ radiation and Hypix-6000HE detector. A single crystal for diffraction measurement was mounted with epoxy resin on a glass fiber, the temperature of which was controlled using a nitrogen gas-flow. The collected X-ray diffraction data were processed using CrysAlisPro. The obtained data were solved with the SHELXT structure solution program and refined with the SHELXL refinement package using Olex2 ver1.5. Hydrogen atoms were refined using the riding model. The powder X-ray diffraction (PXRD) patterns were recorded on a Rigaku SmartLab9kW/IP/HY/N diffractometer using $\text{CuK}\alpha$ radiation ($\lambda = 1.540593 \text{ \AA}$) in the 2θ range of 4° – 40° with a step size of 0.02° and a scan rate of 1° min^{-1} . The sample film was prepared by drop-casting the CHCl_3 solution of **1o** (5.0 mM) on the Si single-crystalline substrate. The simulated PXRD pattern of **1o** was generated from the single-crystal X-ray data using the Free Mercury program by the Cambridge Crystallographic Data Center. The setting wavelength, step size and FWHM (2θ) were 1.54056 Å , 0.02° and 0.34° , respectively.

UV-vis absorption spectral measurements

UV-vis absorption spectra were recorded using a JASCO V-550 or V-760 spectrometer. The decay of the peaks in the visible region by thermal cycloreversion reaction were measured at 90°C in toluene and at 130, 140, 150 and 160°C in decalin. The temperature was controlled by a JASCO ETC 505T temperature controller (90°C), and an aluminium bath and a magnetic stirrer with a hot plate (EYELA RCH-1000) (130, 140, 150 and 160°C).

Quantum yield measurements

The quantum yields of photocyclization and photocycloreversion were measured using a Shimadzu QYM-01. The excitation



wavelength (ϕ_{o-c}/ϕ_{c-o}) was 330/540 nm in CHCl_3 and 365/540 nm in toluene. The change in the absorption spectra and the number of photons absorbed by **1o** and **1c** were measured, then each change of the number of **1o** and **1c** was calculated upon photoirradiation. To reveal the oxygen effect, the CHCl_3 solution of **1** was bubbled with oxygen and nitrogen for 15 min and then the quantum yields were measured respectively.

Emission spectral measurements

Emission and excitation spectra were measured using a JASCO FP-8500 spectrometer. The excitation wavelengths were 350 nm in toluene and 300 nm in PMMA film.

Emission quantum yield measurements

Emission quantum yield was measured using a Hamamatsu Photonics C9920-02 instrument with an integrating sphere. The excitation wavelength was 365 nm in toluene.

Theoretical calculations

The optimized structures of the ground state and molecular orbitals were calculated by the density functional theory (DFT) and time-dependent density functional theory (TD-DFT) method at the $\omega\text{B97XD}/6\text{-}31\text{+G(d)}$ level of theory. NICS(0) values were calculated by the gauge-independent atomic orbital (GIAO method) at the $\omega\text{B97XD}/6\text{-}31\text{+G(d)}$ level of theory. The Banquo atoms were placed on the centroid of rings and the NMR shift was calculated. All calculations were carried out using the Gaussian16 package.⁴⁸

The bowl depth of corannulene moiety

The bowl depth is defined the distance between the centroid of the five interior carbon atoms and the centroid of the ten carbon atoms on the rim.

The isolation of **1c**

The closed form of **1** (**1c**) was isolated by HPLC (CHCl_3 :Hexane = 1:3) from the mixture of **1o** and **1c** obtained by UV-irradiation of the solution of **1o**. HPLC separation was performed with a COSMOSIL 5SL-II packed column (20 mm I.D. \times 250 mm, Nacalai Tesque, Inc.), a UV/vis detector (JASCOUV-2075 Plus) and an HPLC pump (JASCO PU-2080 Plus).

Data availability

The data supporting this article have been included as part of the ESI.† Crystallographic data for **1** has been deposited at the CCDC under 2345853† and can be obtained from DOI: [10.1039/d4tc03157j](https://doi.org/10.1039/d4tc03157j).

Conflicts of interest

There are no conflicts to declare.

Acknowledgements

The authors acknowledge Prof. Masahiro Ehara for his support on the calculation with technical assistance and Ms Yoshiko Nishikawa for her support in the EI mass measurement. This work was partly supported by JSPS KAKEN-HI Grant Numbers JP23H04876 and JP22H05134 for Transformative Research Area (A), and JP24K08361/JP22H02052 for Grant-in-Aid for Scientific Research (C/B) (M. Y./T. K.). This work made use of NAIST common facilities supported by “Advanced Research Infrastructure for Materials and Nanotechnology” in Japan (ARIM) of Ministry of Education, Culture, Sports, Science and Technology (MEXT) (JPMXP1224NR5023). This research was supported by Joint Research by Institute for Molecular Science (IMS) program JPMXP1222MS0016, JPMXP1223MS0021).

Notes and references

- M. Irie, T. Fukaminato, K. Matsuda and S. Kobatake, *Chem. Rev.*, 2014, **114**, 12174.
- In Photosynergetic Responses in Molecules and Molecular Aggregates*, ed H. Miyasaka, K. Matsuda, J. Abe and T. Kawai, Springer, Singapore, 2020.
- G. Berkovic, V. Krongauz and V. Weiss, *Chem. Rev.*, 2000, **100**, 1741.
- B. L. Feringa, *Acc. Chem. Res.*, 2001, **34**, 504.
- D. Bléger and S. Hecht, *Angew. Chem., Int. Ed.*, 2015, **54**, 11338.
- J. Orrego-Hernández, A. Dreos and K. Moth-Poulsen, *Acc. Chem. Res.*, 2020, **53**, 1478.
- S. Pu, T. Yang, J. Xu and B. Chen, *Tetrahedron Lett.*, 2006, **47**, 6473.
- M. Irie, *Chem. Rev.*, 2000, **100**, 1685.
- S. Fukumoto, T. Nakashima and T. Kawai, *Angew. Chem., Int. Ed.*, 2011, **50**, 1565 (*Angew. Chem.*, 2011, **123**, 1603).
- Y.-T. Wu and J. S. Siegel, *Chem. Rev.*, 2006, **106**, 4843.
- J. C. Hanson and C. E. Nordman, *Acta Crystallogr., Sect. B: Struct. Crystallogr. Cryst. Chem.*, 1976, **32**, 1147.
- M. C. Stuparu, *Acc. Chem. Res.*, 2021, **54**, 2858.
- W. E. Barth and R. G. Lawton, *J. Am. Chem. Soc.*, 1966, **88**, 380.
- In Fragments of Fullerenes and Carbon Nanotubes: Designed Synthesis, Usual Reactions, and Coordination Chemistry*, ed M. A. Petrukhina and L. T. Scott, John Wiley & Sons, Hoboken, NJ, 2012.
- R. G. Lawton and W. E. Barth, *J. Am. Chem. Soc.*, 1971, **93**, 1730.
- T. Kawase and H. Kurata, *Chem. Rev.*, 2006, **106**, 5250.
- B. M. Schmidt, S. Seki, B. Topolinski, K. Ohkubo, S. Fukuzumi, H. Sakurai and D. Lentz, *Angew. Chem., Int. Ed.*, 2012, **51**, 11385 (*Angew. Chem.*, 2012, **124**, 11548).
- L. T. Scott, M. M. Hashemi and M. S. Bratcher, *J. Am. Chem. Soc.*, 1992, **114**, 1920.
- A. Sygula, A. H. Abdourazak and P. W. Rabideau, *J. Am. Chem. Soc.*, 1996, **118**, 339.



- 20 T. J. Seiders, K. K. Baldridge, G. H. Grube and J. S. Siegel, *J. Am. Chem. Soc.*, 2001, **123**, 517.
- 21 S. Sanyal, A. K. Manna and S. K. Pati, *ChemPhysChem*, 2014, **15**, 885.
- 22 G. Monaco, L. T. Scott and R. Zanasi, *J. Phys. Chem. A*, 2008, **112**, 8136.
- 23 M. Yamada, T. Sawazaki, M. Fujita, F. Asanoma, Y. Nishikawa and T. Kawai, *Chem. – Eur. J.*, 2022, **28**, e202201286.
- 24 L. K. Sam, T. T. Clikeman, C. Dubceac, A. A. Popov, Y.-S. Chen and M. A. Petrukhina, *Chem. – Eur. J.*, 2015, **21**, 9488.
- 25 M. A. Petrukhina, K. W. Andreini, L. Peng and L. T. Scott, *Angew. Chem., Int. Ed.*, 2004, **43**, 5477.
- 26 S. Kobatake, K. Uchida, E. Tsuchida and M. Irie, *Chem. Commun.*, 2002, 2804.
- 27 M. Nishio, *CrystEngComm*, 2004, **6**, 130.
- 28 D. Xu, Y. Ma, Z. Jing, L. Han, B. Singh, J. Feng, X. Shen, F. Cao, P. Oleynikov, H. Sun, O. Terasaki and S. Che, *Nat. Commun.*, 2014, **5**, 4262.
- 29 J. A. K. Howard, V. J. Hoy, D. O'Hagan and G. T. Smith, *Tetrahedron*, 1996, **52**, 12613.
- 30 P. R. Schleyer, C. Maerker, A. Dransfeld, H. Jiao and N. J. R. E. Hommes, *J. Am. Chem. Soc.*, 1996, **118**, 6317.
- 31 D. Govorov, N. R. Pitawela and A. D. Gudmundsdottir, *J. Phys. Org. Chem.*, 2023, **36**, e4464.
- 32 H. Xu, S. Wei, C. Fan, G. Liu and S. Pu, *Tetrahedron*, 2017, **73**, 6479.
- 33 R. Wang, S. Pu, G. Liu, S. Cui and W. Liu, *Tetrahedron Lett.*, 2012, **53**, 320.
- 34 S. Pu, C. Fan, W. Miao and G. Liu, *Tetrahedron*, 2008, **64**, 9464.
- 35 K. Shibata, S. Kobatake and M. Irie, *Chem. Lett.*, 2001, 618.
- 36 M. Irie and K. Sayo, *J. Phys. Chem.*, 1992, **96**, 7671.
- 37 D. Kitagawa and S. Kobatake, *Chem. Rec.*, 2016, **16**, 2005.
- 38 K. Morimitsu, K. Shibata, S. Kobatake and M. Irie, *J. Org. Chem.*, 2002, **67**, 4574.
- 39 S. Takami, S. Kobatake, T. Kawai and M. Irie, *Chem. Lett.*, 2003, **32**, 892.
- 40 D. Kitagawa, T. Nakahama, Y. Nakai and S. Kobatake, *J. Mater. Chem. C*, 2019, **7**, 2865.
- 41 H. Ishitobi, Z. Sekkat, M. Irie and S. Kawata, *J. Am. Chem. Soc.*, 2000, **122**, 12802.
- 42 S. Long, S. Bi, Y. Liao, Z. Xue and X. Xie, *Macromol. Rapid Commun.*, 2014, **35**, 741.
- 43 A. Monshi, M. R. Foroughi and M. R. Monshi, *World J. Nano Sci. Eng.*, 2012, **2**, 154.
- 44 T. Fukaminato, S. Ishida and R. Métivier, *NPG Asia Mater.*, 2018, **10**, 859.
- 45 S.-C. Pang, H. Hyun, S. Lee, D. Jang, M. J. Lee, S. H. Kang and K.-H. Ahn, *Chem. Commun.*, 2012, **48**, 3745.
- 46 V. Gray, A. Lennartson, P. Ratanalert, K. Börjesson and K. Moth-Poulsen, *Chem. Commun.*, 2014, **50**, 5330.
- 47 R. Asato, C. J. Martin, T. Nakashima, J. P. Calupitan, G. Rapenne and T. Kawai, *J. Phys. Chem. Lett.*, 2021, **12**, 11391.
- 48 M. J. Frisch, G. W. Trucks, H. B. Schlegel, G. E. Scuseria, M. A. Robb, J. R. Cheeseman, G. Scalmani, V. Barone, G. A. Petersson, H. Nakatsuji, X. Li, M. Caricato, A. V. Marenich, J. Bloino, B. G. Janesko, R. Gomperts, B. Mennucci, H. P. Hratchian, J. V. Ortiz, A. F. Izmaylov, J. L. Sonnenberg, D. Williams-Young, F. Ding, F. Lipparini, F. Egidi, J. Goings, B. Peng, A. Petrone, T. Henderson, D. Ranasinghe, V. G. Zakrzewski, J. Gao, N. Rega, G. Zheng, W. Liang, M. Hada, M. Ehara, K. Toyota, R. Fukuda, J. Hasegawa, M. Ishida, T. Nakajima, Y. Honda, O. Kitao, H. Nakai, T. Vreven, K. Throssell, J. A. Montgomery, Jr., J. E. Peralta, F. Ogliaro, M. J. Bearpark, J. J. Heyd, E. N. Brothers, K. N. Kudin, V. N. Staroverov, T. A. Keith, R. Kobayashi, J. Normand, K. Raghavachari, A. P. Rendell, J. C. Burant, S. S. Iyengar, J. Tomasi, M. Cossi, J. M. Millam, M. Klene, C. Adamo, R. Cammi, J. W. Ochterski, R. L. Martin, K. Morokuma, O. Farkas, J. B. Foresman and D. J. Fox, *Gaussian 16 (Revision C.01)*, Gaussian, Inc., Wallingford CT, 2016.

